International Conference on Space Optics—ICSO 2024
Antibes Juan-les-Pins, France
21-25 October 2024

Edited by Philippe Kubik, Frédéric Bernard, Kyriaki Minoglou and Nikos Karafolas

First-light results of the in-orbit demonstration of a CubeSat-compatible optical communication terminal

International Conference on Space Optics — ICSO 2024, edited by Frédéric Bernard, Nikos Karafolas, Philippe Kubik, Kyriaki Minoglou, Proc. of SPIE Vol. 13699, 1369907 · © 2025 ESA and CNES · 0277-786X · doi: 10.1117/12.3075383

First-light results of the in-orbit demonstration of a CubeSat-compatible optical communication terminal

Gert Witvoet[a,b], Dick de Bruijn[c], Stefano Redi[a],
Rodolf W. Herfst[a], and Cornelis W. Korevaar[a,d]

[a]TNO, Optomechatronics department, Delft, The Netherlands
[b]Eindhoven University of Technology, Department of Mechanical Engineering, Control Systems Technology group, Eindhoven, The Netherlands
[c]TNO, Optics department, Delft, The Netherlands
[d]Eindhoven University of Technology, Department of Electrical Engineering, Signal Processing Systems group, Eindhoven, The Netherlands

ABSTRACT

A stable optical link has been established between an in-orbit CubeSat-compatible laser terminal and a low-cost optical ground station in The Hague, and successful 1 Gbps direct-to-earth downlink communication with bit-error-rates down to 10^{-6} has been demonstrated. This paper reports upon the recent developments around both the involved space hardware (CubeCAT) and the ground hardware (GOCAT), developed by TNO and its partners, and describes some of the milestone in-orbit demonstration results to get to this success. The results demonstrate effective feedback control on both ends of the optical link, and reveal interesting variations and similarities in atmospheric conditions between overpasses.

Keywords: Free space optical communication, field test, in-orbit demonstration, cubesats

1. INTRODUCTION

Free-space optical communication (FSOC) harnesses the power of light to transmit data through space, offering breakthrough possibilities for e.g. intersatellite connectivity and direct-to-earth (DTE) applications. FSOC offers a high-speed, secure, and low Size-Weight-and-Power (SWaP) alternative to traditional radio-frequency (RF) communication methods between satellites and ground stations, but comes with specific challenges such as extremely precise pointing in the presence of atmospheric turbulence and platform vibrations.

FSOC is a rapidly evolving field in general, and its application to satellite communication in particular has received significant attention ever since the technology has been demonstrated in space.[1,2] An emerging trend in FSOC is the development of DTE terminals for small low-earth-orbit (LEO) satellites,[3] offering high-speed downlink alternatives for the data generated on the satellite itself. More specifically, one of the recent trends is the focus on demonstrators of potential commercial products with the development of CubeSat-compatible terminals. Examples include the PIXL-1[4] payload from DLR, and the TBIRD[5] payload from NASA. Another example is the CubeSat Communication Active Terminal (CubeCAT),[6,7] developed by TNO and its partners, which is smaller than TBIRD (1U vs 1.8U), offers a higher downlink data rate than PIXL-1 (1Gbps vs 100Mbps), and is capable of actively correcting for satellite body-pointing errors of more than 20 mrad.

CubeCAT has been designed as a generic CubeSat-compatible terminal, with no specific satellite or mission in mind. As such, when an in-orbit demonstration (IOD) opportunity arose, it needed to be extended with an additional suspension module[8] in order to a) interface with the selected NorSat-TD satellite, which is a SmallSat instead of a CubeSat, and b) survive the heavier than anticipated launch loads of the associated Falcon-9 launch platform. This extended version is called SmallCAT, which has been launched onboard the Norsat-TD satellite in April 2023, and successfully went through commissioning.

Further author information: gert.witvoet@tno.nl or wim.korevaar@tno.nl

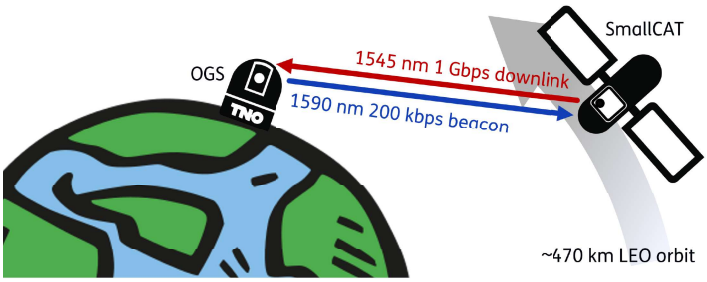

Figure 1. Simple visualization of the presented IOD.

In parallel, TNO has developed the optical ground station (OGS) counterpart,[8] consisting of, among others, an 800 mm telescope, an optical communication bench, and an optical modem, installed on a 45 m tower in The Hague, The Netherlands. Since the SmallCAT launch in April 2023 several optical links have been established between this OGS and SmallCAT, demonstrating successful tracking on both sides. In this paper we will report on the recent developments around SmallCAT and the OGS, and will present some of the most important first-light results of this IOD.

2. DIRECT-TO-EARTH IN-ORBIT DEMONSTRATOR

Recent developments in FSOC aim to further commercialize the technology, which is reflected in the development of various small CubeSat-compatible terminals for direct-to-earth (DTE) applications. Crucial in the push for higher technology readiness level (TRL) of these terminals is the need for actual in-orbit demonstrations (IODs), which is by no means straightforward. Apart from the practical challenges of launching something into orbit, achieving a stable optical link for several minutes over hundreds of kilometers, through a turbulent and often unpredictable atmosphere, requires both ends of the link to function and perform near-perfect.

In this paper we will share updates from TNO's most recent IOD journey, involving SmallCAT as space terminal (which is essentially CubeCAT installed inside a dedicated suspension module) and TNO's optical ground station (OGS) in The Hague as ground-based counter terminal, as illustrated in Fig. 1. Both systems will be further discussed in this paper, and the first-light results obtained with them will be presented.

2.1 Space terminal

The ambition behind the CubeCAT project was to design and realize a generic commercially viable compact DTE space terminal that could fit onto any CubeSat. To this end, the design target was to fit *all* functionality, i.e. the complete optical bench, laser and laser driver, modem and all other electronics, inside a very tight 1U volume of 10 cm × 10 cm × 10 cm. Moreover, it has been designed to provide a 1 Gbps downlink channel, and it was decided to rely on a 200 kbps 1590 nm wavelength uplink beacon signal, not only to let CubeCAT determine its tracking error in real time, but also to provide a slow uplink connection, meant to upload small commands and settings at later stages.

Since CubeCAT originally wasn't designed for a specific satellite or mission, it was desired to make CubeCAT as versatile as possible. Hence, in the absence of any satellite body pointing specifications, or information on interface tolerances or launch loads, it was decided to design CubeCAT such that it would have a relatively large field-of-view (FoV) and would have means to actively compensate for errors and misalignments of up to about ±1°. Early link budget calculations motivated the choice for a 17 mm aperture, implying that CubeCAT should be able to meet its pointing requirement of about 50 µrad 3σ with beacon intensities at aperture of only 1.8 nW (translating to worst-case intensity of only 0.8 nW at the tracking sensor).

2.1.1 CubeCAT optical bench

The heart of CubeCAT is formed by the optical bench, a picture of which is shown in Fig. 2(a). This picture was taken during assembly, and highlights some of the critical components. The received Rx beacon enters through the 17 mm baffle aperture on the right, and is then reflected off the Fine Steering Mirror (FSM) towards

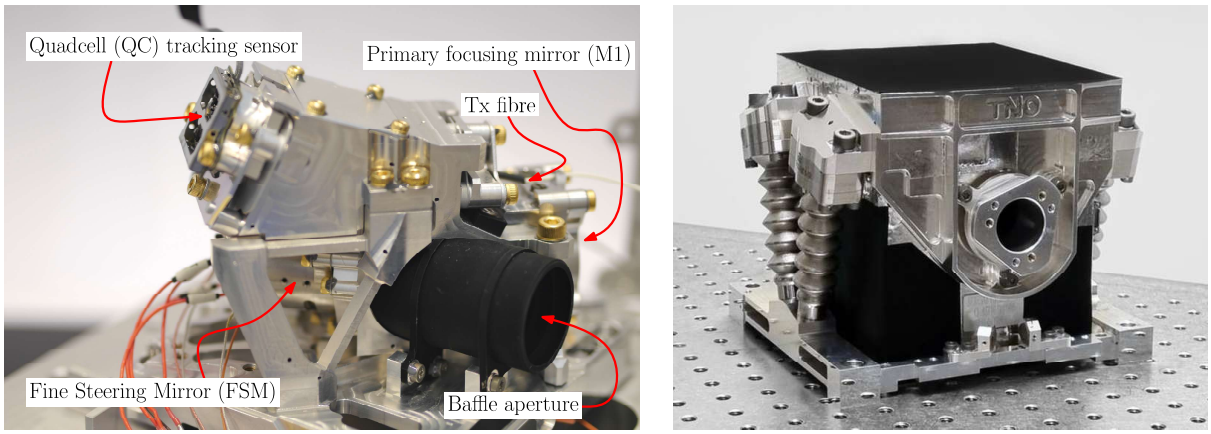

(a) The optical bench during assembly, highlighting, among others, the locations of the FSM and the QC.

(b) SmallCAT flight model, just before installation on the satellite.

Figure 2. Pictures of the SmallCAT hardware.

the parabolic primary mirror (M1), which then focuses the light towards the quadcell (QC), which acts as the tracking sensor. Inside the aluminium housing is a beamsplitter which couples the light of the Tx fibre onto the same optical path as the Rx, leaving the aperture via the same FSM. Due to this common-path approach any angle between the Rx beacon and the terminal boresight will show up as a spot displacement on the tracking sensor, which is then corrected for by the FSM via a feedback loop, so as to point the Tx exactly in the same direction as the Rx beacon. CubeCAT does not have a separate point-ahead mirror (PAM); point-ahead angles between Rx and Tx are obtained by controlling towards a small offset on the QC.

The FSM[9] used in CubeCAT is a TNO-designed mechanism,[10,11] manufactured by Demcon, capable of providing $\pm 1°$ mechanical tip/tilt of a 20 mm diameter flat mirror, using a variable reluctance actuator concept.[10,11] This efficient actuation concept allows for a relatively small size, weight and power (SWaP) of the FSM, which proved to be essential in meeting the 1U volume constraint of CubeCAT. The FSM is actuated by PWM currents, generated by a custom-designed driver by AAC Hyperion, while no internal FSM metrology is used.

The QC electronics is also a dedicated design by AAC Hyperion, focused on keeping the volume, latency and tip/tilt sensor noise as low as possible. To this end it mixes the measured analog intensities on the four QC quadrants with an internal 100 kHz clock, so as to lock on the 200 kbps beacon, and then combines, filters and downsamples the signals to generate 20 kHz tip/tilt information for the feedback loop. Due to this locking the sensor is relatively insensitive to DC background signals from e.g. sunlight and albedo. The QC itself is placed slightly out-of-focus for an optimal balance between sensitivity and linearity of its response. Tests demonstrated that this gives CubeCAT a total FoV of about ± 6 mrad, of which the central ± 0.6 mrad is approximately linear. The QC electronics was designed to also decode the 200 kbps data on the beacon, but this functionality is not yet implemented on the current version.

The CubeCAT Tx beam has a divergence of 85 µrad half-angle; its source was provided by Gooch&Housego, which delivers a 1545 nm wavelength 300 mW Tx laser. Given the objectives of the IOD and the tight time schedule of the launch opportunity, it was decided to program the laser driver, provided by AAC Hyperion, such that it repeatedly modulates the Tx beam with a known PRBS-23 sequence, which allows for easy bit-error-rate (BER) verification calculations at the OGS.

2.1.2 Feedback control and acquisition

Accurate Tx pointing of CubeCAT is enabled by the fine pointing feedback loop between QC and FSM. A dedicated real-time control algorithm has therefore been developed, which runs with a fixed 20 kHz rate on a small processor board within the same 1U volume. This algorithm was carefully designed based on link budgets and QC noise measurements, guaranteeing sufficient pointing accuracy even in the case of expected

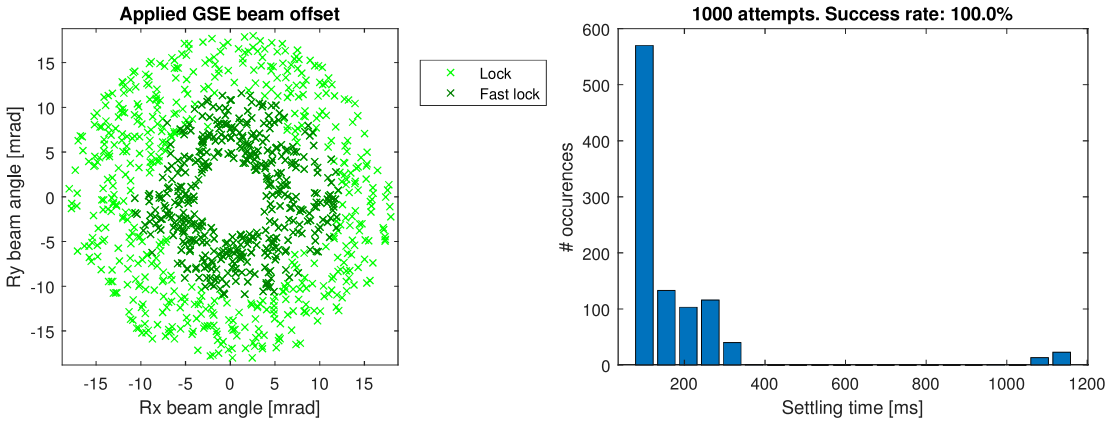

Figure 3. Summary of 1000 acquisition tests, where each cross in the left plot represents a test with a random initial angle-of-arrival error of up to 18 mrad; dark green indicates an immediate successful acquisition without spiraling, light green a somewhat slower acquisition needing some level of spiraling, and red (which are absent) an unsuccessful acquisition. The right plot shows an histogram of the associated acquisition times of all 1000 tests, where the settling time is stringently defined by how long it takes for the pointing error to stay within just ±40 µrad.

minimal beacon intensity (and hence maximal sensor noise). As such the effective control bandwidth was set conservatively at about 60 Hz; note that the high 20 kHz sample rate, together with the possibility to upload new controller settings while in orbit, allow for further enhancements later on in case the IOD results would give reason to do so.

Microvibrations can have a strong effect on Tx pointing, but are often hard to quantify *a priori*. Therefore, in the absence of vibration requirements, for CubeCAT it was decided to specify an allowable satellite motion which could still be sufficiently suppressed by the feedback loop. Based on the above 60 Hz bandwidth controller, this was determined to be 1.9 mrad/s root-mean-square (rms) motion for frequencies up to 120 Hz, and 2.5 µrad rms motion for higher frequencies. The NorSat-TD satellite, that was later selected as IOD platform (see Sec. 2.1.3), was assessed to be compliant with both.

Apart from feedback control, the real-time algorithm also provides CubeCAT with additional in-orbit functionality, including dynamic system identification, dealing with fades, Rx/Tx re-alignment and scanning acquisition. Although the CubeCAT FoV of ±6 mrad should be large enough to cover all uncertainties and expected body pointing errors, avoiding the need for an explicit acquisition routine, the latter functionality provides a backup acquisition scenario by quickly spiraling the FSM in open loop. This effectively enlarges the FoV, and thus robustness for misalignments and uncertainties, to more than 20 mrad. This is illustrated by the laboratory results shown in Fig. 3, showing successful acquisition tests with 1000 different random initial angle-of-arrivals of the beacon of up to 18 mrad. The plots show that the vast majority of these tests settle without spiraling within 75 ms to an error of less than ±40 µrad, many others need at most 350 ms to settle after some level of spiraling, while only a few need a little more than one complete spiral to successfully lock, and none of them fail.

Finally, the control processor board, supplied by AAC Hyperion, also has the ability to trace and log a number of important variables in the algorithm with the same 20 kHz rate. This has proven to be a very useful functionality during commissioning, debugging and testing after launch. Unfortunately, due to practical limitations, so far it has only been possible to download about 20 s of tracing data per satellite overpass of several minutes. This 20 s tracing window does not always align with the establishment of an optical link, which means that not every successful link also provided useful tracing data.

2.1.3 From CubeCAT to SmallCAT

Although designed for generic CubeSats, the launch opportunity that arose for CubeCAT's IOD was on-board the NorSat-TD SmallSat. Not only did this introduce a different interface, the NorSat-TD would be launched with a Falcon-9 carrier, which would provide higher launch loads than anticipated. Since the design was nearly finished

Figure 4. Pictures of the TNO OGS facility in The Hague, showing the tower with the dome on top (left), the opened dome (top right) and the ASA telescope inside the dome (bottom right).

by then, and it was desired to keep the CubeSat-compatibility in tact, it was therefore decided to design and manufacture an additional mounting interface with integrated suspension.[8] The CubeCAT terminal mounted inside this suspension is referred to as SmallCAT, a picture of which is shown in Fig. 2(b). The suspension module encompasses six tailor-designed 3D-printed metal struts with integrated viscoelastic rubber. These dampers operate hysteresis-free and are tuned for a specific eigenfrequency with significantly increased damping, thereby reducing the impact of random vibration loads while keeping the alignment between the mechanical interface and the SmallCAT boresight deterministic.

Originally, thermal straps[8] were foreseen on the suspension module to flow away heat dissipated on CubeCAT by e.g. the laser and the electronics. However, early vibration tests revealed that these straps introduced too much stiffness for the suspension to work properly. Thermal analyses then showed the feasibility of heat radiation, provided that CubeCAT would be a sufficiently black body. As such, the thermal straps have been removed from SmallCAT, and it has been taped with coated black foil, as is visible in Fig. 2(b). SmallCAT then successfully went through vibration and thermal cycling tests before integration on NorSat-TD. NorSat-TD has been launched and successfully released into orbit on April 15, 2023. It is now in a sun-synchronous low-earth orbit (LEO) around the earth at an altitude of about 470 km.

2.2 Optical Ground Station (OGS)

For the other end of the FSOC IOD, TNO has created its own OGS facility in The Hague, The Netherlands, pictures of which are shown in Fig. 4. On the rooftop of a 45 m high former RF-tower a dome has been installed, inside which an 800 mm ASA telescope has been installed to perform the coarse tracking of the NorSat-TD satellite. The telescope is controlled with a DiGOS SCOPE based system, and a Miratlas Integrated Sky Monitor is installed on the tower rooftop to measure turbulence conditions.

To be able to establish an optical link with SmallCAT, the Gigabit Optical Communication Active Terminal (GOCAT) has been developed. GOCAT is an optical ground terminal that can be mounted onto the OGS

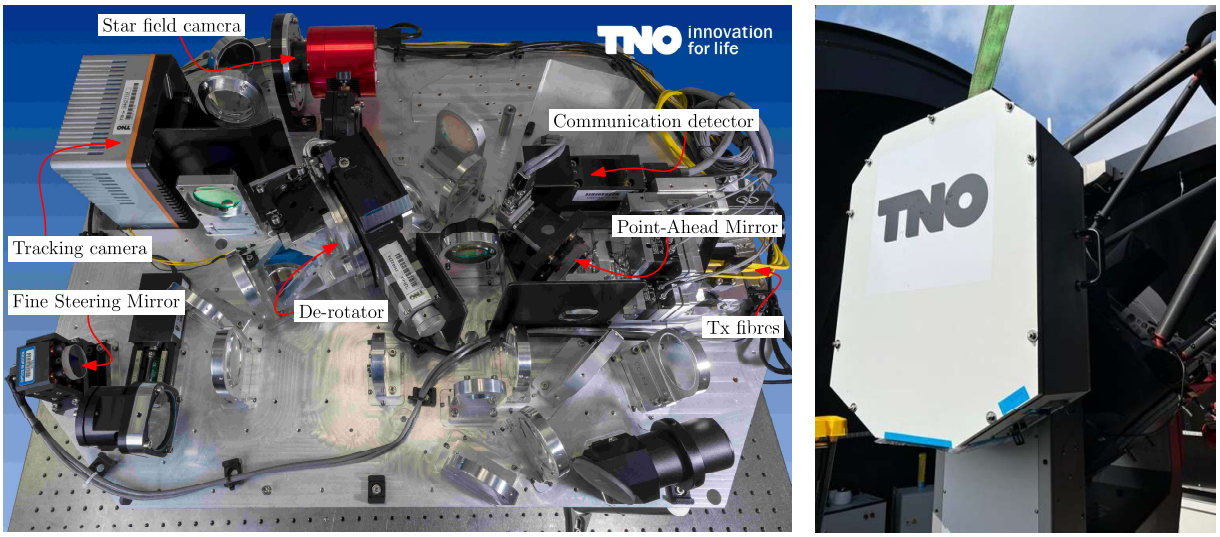

Figure 5. Pictures of GOCAT, the communication terminal in the OGS; the optical bench during testing in the lab (left), and the complete GOCAT unit installed on the nasmyth platform of the telescope (right).

telescope, designed for bi-directional communication links to a LEO satellite, capable of data rates up to 10 Gbps. It has been developed in collaboration with Airbus-NL, with the aim of demonstrating the feasibility of a low-cost gigabit ground terminal, and as such utilizes as much commercial-off-the-shelf components as possible. The picture on the right of Fig. 5 shows the GOCAT unit after installation on the nasmyth platform of the OGS telescope.

A picture of the GOCAT interior, i.e. the optical bench, is shown on the left of Fig. 5, highlighting some of its most important components. The Rx light from the nasmyth port of the telescope enters from the bottom, through the middle, and is then reflected through the de-rotator (to correct for the telescope rotation) onto the FSM. The light is then split partly towards the tracking camera, and partly to the communication detector. The Tx light is reflected off a point-ahead mirror, before following a largely similar path back into the telescope. A separate real-time computer closes the loop between camera and FSM, and commands the PAM and the de-rotator, in order to establish the fine pointing towards the satellite.

GOCAT is designed to support four Tx laser beams of 10 W each, distributed along the aperture of the telescope (positioned such that there is no obscuration due to the telescope spider), and therefore is equipped with four Tx fibres. However, during the IOD only one 6 W laser source was available. GOCAT is designed to receive a 1545 nm wavelength Rx downlink, and provides a 100 kHz modulated 1590 nm wavelength Tx uplink, and is therefore compliant with SmallCAT. The Tx has a 220 µrad half-angle divergence, and can furthermore be spiraled during acquisition via the PAM.

It should be noted that one of the challenges in operating the OGS turned out to be the coarse pointing of the telescope. For every overpass the telescope should follow a *predefined* trajectory to aim towards the position where the satellite is expected to be, but the match between this prediction and reality obviously highly depends on the timing accuracy and quality of the orbital predictions itself. Therefore, lots of effort went into improving our orbital prediction models; in the end, the best results were obtained by using Consolidated Prediction Format (CPF) files based on satellite GPS data no older than 12 hours. Using this approach consistent telescoping tracking results have been obtained for both day- and night-time overpasses.

3. FIRST-LIGHT RESULTS

After the NorSat-TD launch in April 2023, both SmallCAT and GOCAT went through a commissioning phase; the first attempts to actually establish a link started in July 2023. Ever since, many problems were solved, bugs were fixed, lessons were learned, and improvements were implemented. And there needed to be quite some

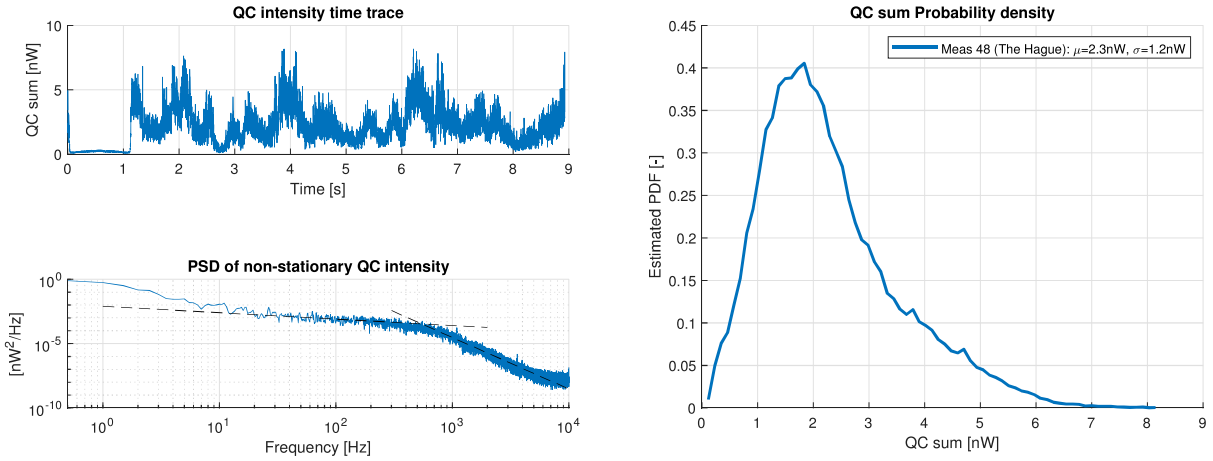

Figure 6. Recorded QC intensity during mission 473161, in which the OGS beacon was first detected, both represented as time trace (top left), PSD (bottom left) and PDF (right). The first second of data is affected by a minor data logging issue and is therefore omitted from the PSD and PDF analyses.

waiting for clear skies, which can sometimes take a few weeks in Dutch weather. This explains the sometimes large gaps in time in the results we will present next. Note also that the reported mission numbers are *not* indicative for the amount of link attempts in between.

3.1 August 22, 2023 (mission 473161): OGS beacon detected on SmallCAT

In the first few weeks of testing it was decided to keep the SmallCAT laser off, and first focus on getting the OGS coarse pointing and satellite tracking right. The success of an attempt was assessed in post-processing afterwards; firstly by comparison of the predicted and tracked satellite orbit with the actual GPS data, and secondly by downloading and analyzing the short high-speed SmallCAT time trace. The first success was recorded on August 22, 2023, when this tracing file revealed that the OGS beacon had been observed, as can be seen in the top left plot in Fig. 6, showing the total intensity on the QC, which is clearly scintillated due to atmospheric effects. This 9 s trace was captured around culmination, at a maximum elevation of a little more than 31°. During this overpass the SmallCAT pointing feedback loop was switched off, hence neither SmallCAT nor OGS were in closed loop. The detection of the OGS beacon thus confirmed that both the coarse pointing of the OGS and the body pointing of NorSat-TD were sufficiently good. Fig. 6 also shows the calculated probability density function (PDF) of the QC intensity on the right, and the power spectral density (PSD) on the bottom left; the first resembles a log-normal distribution,[12] which was expected as it approximates a gamma-gamma distribution for weak turbulence conditions, whereas the second shows a relatively high frequency content, with a cut-off frequency* of a few hundred Hz.

3.2 September 10, 2023 (mission 475042): SmallCAT laser observed on OGS

After this first success, it was decided to turn on both the laser and the feedback loop on SmallCAT for all subsequent overpasses. Two weeks later, on September 10, this resulted in the first detection of the SmallCAT laser on the OGS. Unfortunately, this success was not captured in the SmallCAT tracing file, which recorded ∼20 s of data around culmination (with a maximum elevation of 86°) showing no beacon signal at all, since the lock only happened near the end of the overpass (around an estimated elevation of 25°). As such, although there was a strong indication that the SmallCAT feedback performed properly, this could not be fully confirmed yet. Moreover, on the OGS there was no data logging implemented yet, so the only real proof of this success is the photo of the OGS camera image in Fig. 7, showing the sudden appearance of the SmallCAT laser.

*The PSD of Fig. 6 shows a clear transition from a moderate low-frequency slope to a steep high-frequency slope, highlighted by the indicative black dashed lines fitted through the spectral data. Here we loosely define cut-off frequency as the intersection of these approximate slopes.

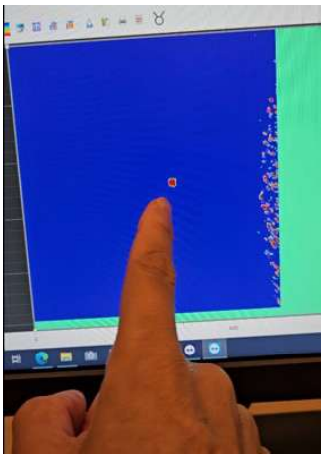

Figure 7. Photo of the OGS camera image at the end of mission 475042, showing the received SmallCAT laser for the first time.

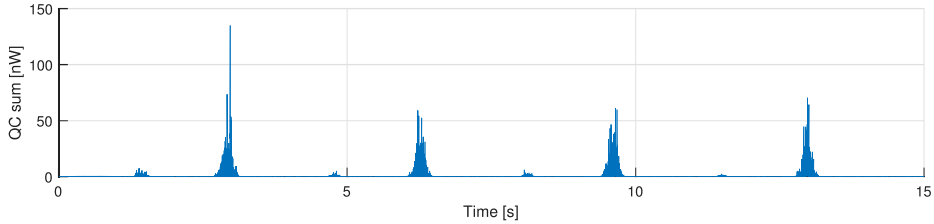

Figure 8. Recorded QC intensity during mission 476323, showing regular blips of the spiraling OGS beacon passing by. Note that the OGS beacon does not spiral inwards; the PAM returns to its zero position as soon as the maximum radius is achieved, then to start the next outward spiral again.

3.3 September 26, 2023 (mission 476323): OGS spirals observed by SmallCAT

The previous successes happened to occur at relatively low elevations; at that time it was therefore assumed that the OGS telescope pointing was not accurate enough to succeed at higher elevations, when pointing accuracies are more critical due to the larger relative velocity of the satellite. It was therefore decided to use an active acquisition scenario for the next attempts by spiraling the PAM outwards to a maximum radius of 350 µrad, effectively increasing the OGS search cone from 220 µrad (its divergence) to 570 µrad half-angle.

This spiraling behavior was later nicely caught in the SmallCAT tracing file on September 26, shown in the time trace of the QC intensity in Fig. 8. This trace shows a repeating sequence of a small and a big blip, demonstrating how the OGS is illuminating SmallCAT twice every spiral. It should be noted that the SmallCAT feedback control was active during this overpass, meaning that the SmallCAT laser was pointed back in the direction of the received beacon every time a blip passed by. The SmallCAT laser has indeed been observed by the OGS (again not logged though), but unfortunately the OGS feedback loop could not be closed back then, thanks to which it kept on spiraling.

That performing IOD tests comes with unexpected challenges was proven in the weeks thereafter, when the OGS tower was struck by a fly plague. One week after the previous overpass, the telescope dome was suddenly filled with thousands of small flies, covering the telescope optics and surrounding equipment, preventing any new link attempts. It took several weeks to get rid of the flies sufficiently, after which we had to wait a few more weeks for the Dutch autumn and winter to give us cloudless weather.

3.4 January 10, 2024 (mission 605068): Both SmallCAT and OGS in feedback

The waiting paid off with some clear winter skies in January 2024, enabling the next breakthrough result on January 10, shown in Fig. 9. During an overpass with 56° maximum elevation, the 17 s SmallCAT tracing file exactly captured the switch from open to closed loop which occurred before culmination at around 44° elevation.

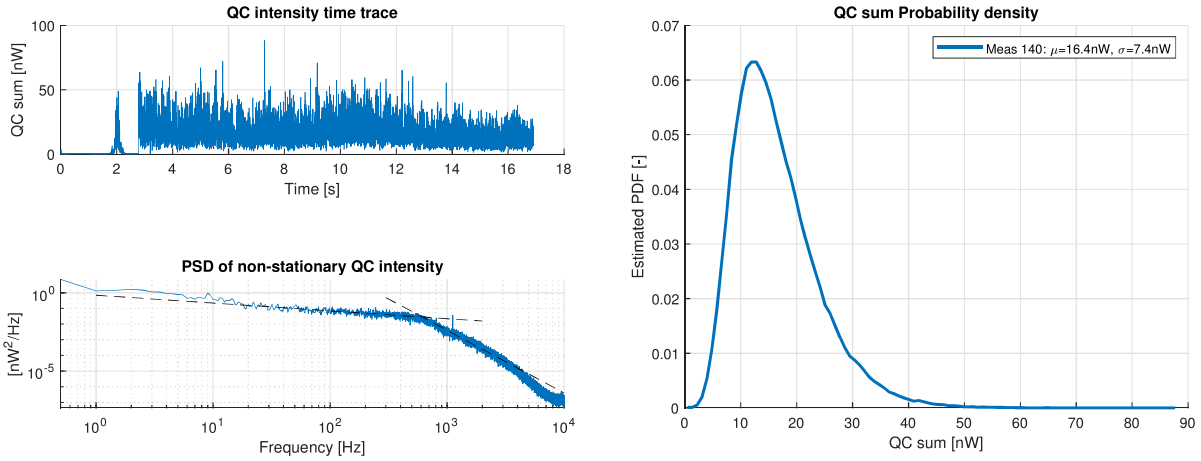

(a) QC intensity (top left), and its PSD (bottom left) and PDF (right).

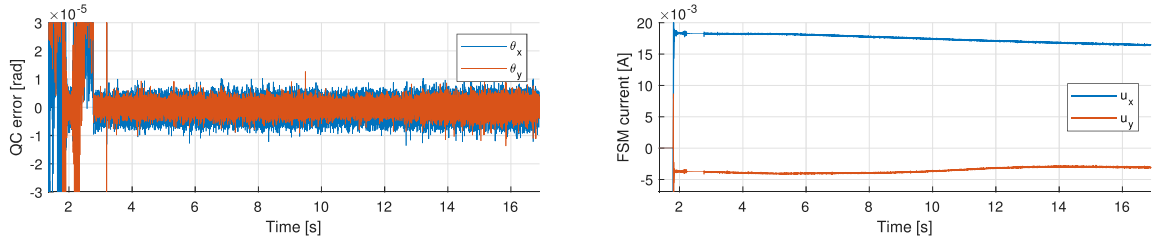

(b) Feedback error as measured by the QC in both tip θ_x and tilt θ_y (left) and the resulting closed-loop currents u_x and u_y sent to the FSM (right).

Figure 9. Recorded SmallCAT time traces of mission 605068 (17 s at 20 kHz).

This can clearly be seen in the top left plot in Fig. 9(a) and the zoomed-in time traces of the QC feedback error and FSM currents in Fig. 9(b). After first receiving no beacon signal at all, there was a sudden blip on the QC intensity around $t = 2\,\mathrm{s}$ due to the spiraling of the OGS. SmallCAT immediately closed its feedback loop, resulting in very rapid FSM angle adjustments indicated by the rapid evolution of the FSM currents u_x and u_y. Although the OGS shortly detected the SmallCAT laser then, it first finished its spiral; this caused SmallCAT to loose beacon signal, but it kept its FSM currents constant and thereby continued to point its laser roughly towards the OGS. Soon thereafter, around $t = 3\,\mathrm{s}$, the OGS stopped its spiral and steered its FSM towards the angle it saw the SmallCAT laser. From that point onward, SmallCAT remained in closed loop for several minutes, causing the OGS to see the SmallCAT laser for several minutes, allowing it to also close its own feedback loop from the camera to the FSM. As such, a stable optical link has been established for several minutes, i.e. a significant part of the overpass, in which even the communication detector of the OGS detected the SmallCAT laser for several minutes.

The received QC intensity is significantly higher than observed before, which is assumed to be caused partly by the higher elevation during tracing (atmospheric disturbances are known to be smaller for higher elevations, leading to less power loss and scintillation), and partly by the fact that both ends of the link have now been in feedback, thereby reducing mispointing and beam wander. The PDF in Fig. 9(a) again shows a close-to log-normal distribution, with a mean received power of 16.4 nW and a standard deviation of 7.4 nW. Interestingly, the PSD in Fig. 9(a) seems to have a similar shape as in Fig. 6 though, again with a cut-off frequency[†] of a few hundred Hz. Note also how the FSM currents are slowly evolving in time, to compensate for the slowly evolving coarse body pointing error of the satellite.

[†]The intersection of the fitted black dashed lines in Fig. 9(a) again loosely defines the cut-off frequency. Their slopes are the same as in Fig. 6, but they differ in magnitude; still the cut-off frequency is roughly the same as in Fig. 6.

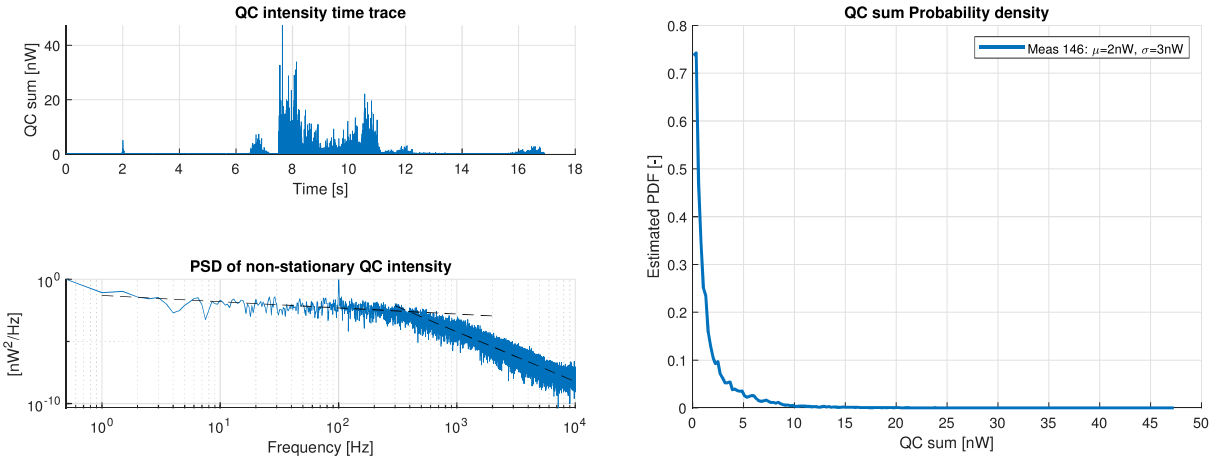

Figure 10. Recorded QC intensity during mission 619062. The time trace (top left) shows numerous long and deep fades, presumably due to quite severe atmospheric conditions. The corresponding PSD (bottom left) and PDF (right) are calculated using only the information between $t = 7.5\,\mathrm{s}$ and $t = 11\,\mathrm{s}$.

Note that the high QC intensity during the link implies that the sensor noise on θ_x and θ_y in the left of Fig. 9(b) is fairly low in this time trace. As such, the mean jitter on this measured QC tip/tilt is a strong indicator of the actual SmallCAT pointing jitter, which is only 2.4 µrad in closed loop, which is much smaller than designed for. This obviously does not necessarily say anything about the *absolute* pointing accuracy of SmallCAT, as e.g. possible Rx/Tx misalignments are not observed by the QC. In future tests quantification and correction of such pointing errors will be attempted.

3.5 January 19 & 22, 2024 (missions 619062 & 622313): Downlink communication

The previous test was a milestone in the sense that it demonstrated a stable optical link between SmallCAT and the OGS for the first time, but there was no oscilloscope or data logger connected to the OGS communication detector yet to actually analyze the downlink communication itself. This high-speed oscilloscope was installed a few days later, and on January 19 this led to the first communication results.

The atmospheric conditions during this 44° maximum elevation overpass were much worse than before, as can be seen in the SmallCAT trace and its PDF shown in Fig. 10; the QC only saw short bursts of beacon light of low intensities, being accommodated by many long and deep fades, resulting in a more exponential PDF (i.e. a gamma-gamma distribution in strong turbulence conditions). Still, these occasional beacon blips helped SmallCAT to steer its laser roughly in the direction of the OGS, which caused the OGS to successfully detect the SmallCAT laser for significant parts of the overpass. Note that the PSD again shows a cut-off of a few hundred Hz; it is now assumed that this high frequency content in all presented traces is predominantly caused by the satellite velocity, and not so much by atmospheric conditions itself.

The OGS communication detector regularly received sufficient light to analyze the bit stream with the oscilloscope, as depicted in Fig. 11(a). This figure shows a snapshot of the detected and expected 1 Gbps PRBS-23 downlink signal (left), in which the bits can clearly be distinguished; the top right image shows the associated eye-diagram, which shows a clear opening. The bottom right figure depicts the determined bit-error rate (BER) for several batches of data during the complete overpass, in which the severe atmospheric conditions can also be observed; BER values of down to 10^{-4} are obtained, but the BER also regularly increases back to 0.5 when the pointing accuracy on either end of the link drops due to long and deep fades (or possibly even clouds). Note that Fig. 10 already showed that these fades could last several seconds, during which SmallCAT and GOCAT essentially fall back to open-loop pointing, which is not accurate enough to couple sufficient light into the communication detector. Both systems can automatically restore closed-loop operation after a fade though, improving pointing, detector coupling and BER values automatically again.

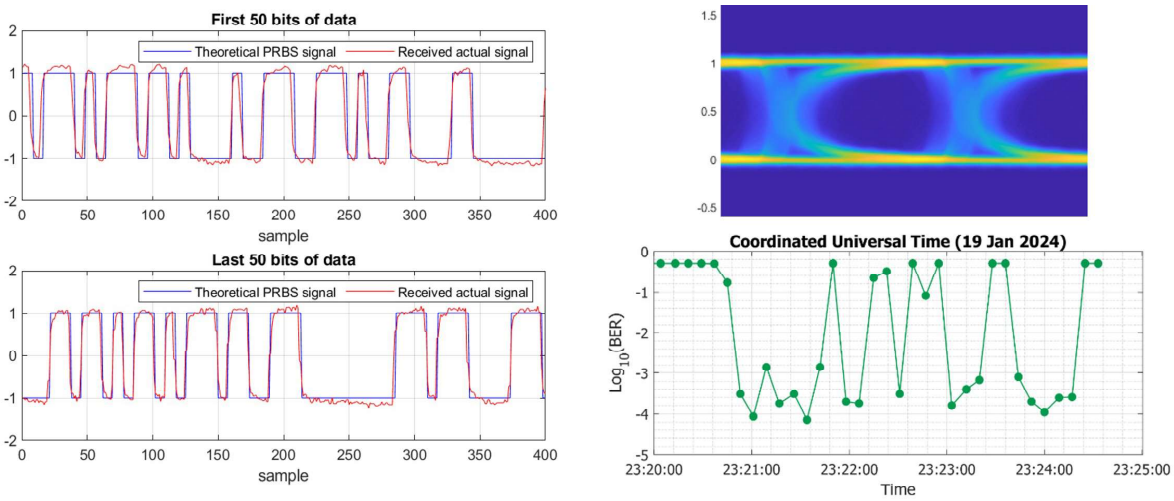

(a) For January 19, 2023 (mission 619062)

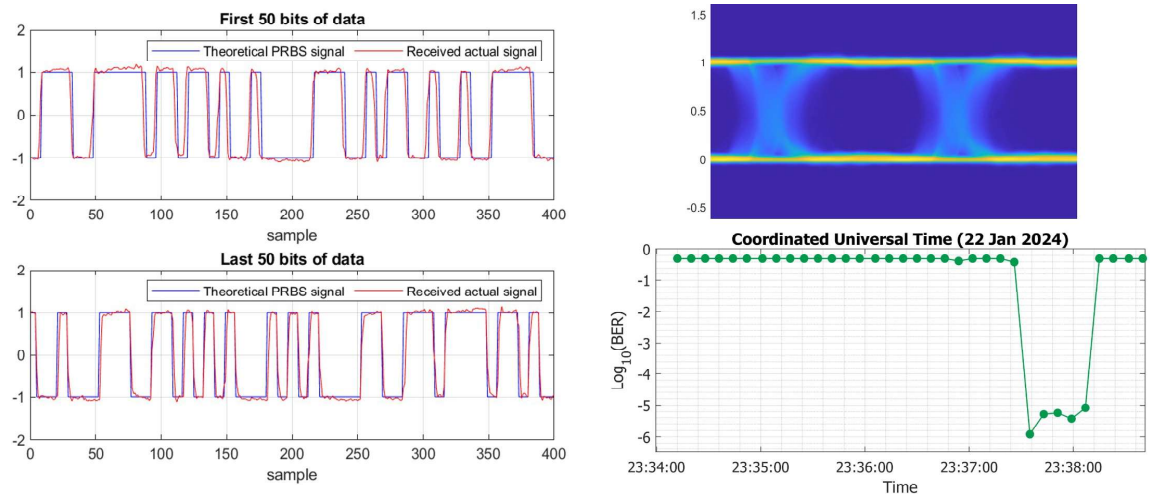

(b) For January 22, 2023 (mission 622313)

Figure 11. Recorded communication results by the OGS for two subsequent successful overpasses. Left: snapshots of the detected bits in relation to the expected PRBS-23 signal; top right: the corresponding eye-diagram; bottom right: the evolution of the effective bit-error-rate (BER) during the overpass.

The same test has been repeated a few days later, on January 22, yielding the results in Fig. 11(b), again returning clear eye-diagrams. In this case it took a bit longer for the link to be established (the maximum elevation was only 32°), but once succeeded consistent BER values between 10^{-6} and 10^{-5} have been achieved for the rest of the overpass.

4. CONCLUSIONS

This paper discussed the recent development of a CubeSat-compatible DTE terminal and its ground-based counterpart by TNO, and presented the first IOD results obtained. Insights and details have been shared around the design and realization of both the CubeCAT/SmallCAT space terminal, and the GOCAT-based OGS in The Hague. The presented IOD test results, over a time frame of about half a year, highlight the difficulty and complexity of establishing a stable optical link and demonstrating downlink communication. Several boxes need

to be ticked for this to happen, which were indeed subsequently tackled in the IOD tests:

- ✓ Sufficiently accurate open-loop orbital tracking by OGS achieved (i.e. OGS beacon detected on SmallCAT);
- ✓ Feedback loop successfully closed on SmallCAT;
- ✓ SmallCAT laser detected on the OGS camera;
- ✓ Feedback loop successfully closed on OGS;
- ✓ SmallCAT laser effectively coupled into OGS detector;
- ✓ Downlink data transmission demonstrated by connecting high-speed oscilloscope to the OGS.

In the end, this has led to the first stable optical link, with active feedback on both ends of the link, on January 10, 2024, and the first downlink communication demonstration on January 19, 2024. Ultimately, BER values down to 10^{-6} with a 1 Gbps downlink have been achieved, which highlights the success of this IOD and the capabilities of the first CubeCAT demonstrator.

The first results also give some early insights in the variations and similarities of the atmospheric conditions. Whereas the PDF of the received beacon signal varies quite significantly between overpasses, even changing from log-normal to exponential distributions, the spectral densities seem to remain fairly constant with high cut-off frequencies. The latter can most likely be attributed to the contribution of the satellite velocity, translating to a large apparent wind speed, which presumably has a much bigger influence on the PSD of the received beacon signal than the atmosphere itself. TNO will continue to try to establish more optical links to gather more data, which can be analyzed to learn more about the performance of both CubeCAT and GOCAT, and the influence of the atmospheric turbulence on the results. There are also ongoing initiatives to attempt to create optical links with different ground stations, which will generate new data and presumably new insights.

ACKNOWLEDGMENTS

TNO would like to explicitly thank its partners, without whom this demonstration and the subsequent results would not have been possible. For the OGS this includes Airbus-NL, ASA, DiGOS and Celestia-STS. Regarding SmallCAT this includes AAC Hyperion and Gooch&Housego for their contribution to the hardware, and NOSA, StatSat and UTIAS-SFL for the launch opportunity and mission support. SmallCAT is supported by the Netherlands Space Office (NSO) and the Netherlands Ministry of Defence, and jointly funded by ESA's ARTES Strategic Programme Line ScyLight and TNO, together with the companies involved in the project.

REFERENCES

[1] Boroson, D. M., Robinson, B. S., Murphy, D. V., Burianek, D. A., Khatri, F., Kovalik, J. M., Sodnik, Z., and Cornwell, D. M., "Overview and results of the lunar laser communication demonstration," in [*Free-Space Laser Communication and Atmospheric Propagation XXVI*], Hemmati, H. and Boroson, D. M., eds., **8971**, 89710S, International Society for Optics and Photonics, SPIE (2014).

[2] Gregory, M., Heine, F., Kämpfner, H., Meyer, R., Fields, R., and Lunde, C., "TESAT laser communication terminal performance results on 5.6Gbit coherent inter satellite and satellite to ground links," in [*International Conference on Space Optics — ICSO 2010*], Armandillo, E., Cugny, B., and Karafolas, N., eds., **10565**, 105651F, International Society for Optics and Photonics, SPIE (2010).

[3] Kolev, D., Carrasco-Casado, A., Trinh, P., Shiratama, K., Ishola, F., Kotake, H., Nakazono, J., Saito, Y., Kunimori, H., Kubooka, T., Tsuji, H., and Toyoshima, M., "Latest developments in the field of optical communications for small satellites and beyond," *Journal of Lightwave Technology* **41**(12), 3750–3757 (2023).

[4] Schmidt, C., Rödiger, B., Rosano, J., Papadopoulos, C., Hahn, M.-T., Moll, F., and Fuchs, C., "DLR's optical communication terminals for CubeSats," in [*2022 IEEE International Conference on Space Optical Systems and Applications (ICSOS)*], 175–180 (2022).

[5] Schieler, C. M., Riesing, K. M., Bilyeu, B. C., Robinson, B. S., Wang, J. P., Roberts, W. T., and Piazzolla, S., "TBIRD 200-Gbps CubeSat downlink: System architecture and mission plan," in [*2022 IEEE International Conference on Space Optical Systems and Applications (ICSOS)*], 181–185 (2022).

[6] Dresscher, M., Korevaar, C. W., van der Valk, N., de Lange, T. J., Saathof, R., Doelman, N., Crowcombe, W., Duque, C., de Man, H., Human, J., Witvoet, G., van der Heiden, N., den Breeje, R., Kuiper, S., and Fritz, E., "Key challenges and results in the design of CubeSat laser terminals, optical heads and coarse pointing assemblies," in [*2019 IEEE International Conference on Space Optical Systems and Applications (ICSOS)*], 1–6 (2019).

[7] Saathof, R., Kuiper, S., Crowcombe, W., de Man, H., de Lange, D., van der Valk, N., Kramer, L., and Fritz, E., "Opto-mechatronics system development for future intersatellite laser communications," in [*Free-Space Laser Communications XXXI*], Hemmati, H. and Boroson, D. M., eds., **10910**, 109101B, International Society for Optics and Photonics, SPIE (2019).

[8] Saathof, R., Meskers, A. J., van Kempen, F., Witvoet, G., Korevaar, W., de Lange, D., Crowcombe, W., Fritz, E., and van de Pol, M., "In orbit demonstration plans for an optical satellite link between a CubeSat and a ground terminal at TNO," in [*Free-Space Laser Communications XXXIII*], Hemmati, H. and Boroson, D. M., eds., **11678**, 1167809, International Society for Optics and Photonics, SPIE (2021).

[9] Milaševičius, M. and Mačiulis, L., "A review of mechanical fine-pointing actuators for free-space optical communication," *Aerospace* **11**(1), 5 (2024).

[10] Kuiper, S., Crowcombe, W., Human, J., Dekker, B., Nieuwkoop, E., Meskers, A., Witvoet, G., Kramer, L., Lemmen, M., Lagemaat, H., van der Hoogt, W., and van Koppen, M., "High-bandwidth and compact fine steering mirror development for laser communications," in [*17th European Space Mechanisms and Tribology Symposium*], (2017).

[11] Witvoet, G., Kuiper, S., and Meskers, A., "Performance validation of a high-bandwidth fine steering mirror for optical communications," in [*International Conference on Space Optics — ICSO 2018*], Sodnik, Z., Karafolas, N., and Cugny, B., eds., **11180**, 1118061, International Society for Optics and Photonics, SPIE (2019).

[12] Wayne, D. T., Phillips, R. L., Andrews, L. C., Leclerc, T., Sauer, P., and Stryjewski, J., "Comparing the Log-Normal and Gamma-Gamma model to experimental probability density functions of aperture averaging data," in [*Free-Space Laser Communications X*], Majumdar, A. K. and Davis, C. C., eds., **7814**, 78140K, International Society for Optics and Photonics, SPIE (2010).